Secondary electron emission due to multi-species iodine ion bombardment of different target materials

L. Habl, D. Rafalskyi, T. Lafleur

Secondary electron emission due to multi-species iodine ion bombardment of different target materials

L. Habl,[1, 2, a)] D. Rafalskyi,[2] and T. Lafleur[2]
[1)]*Laboratoire de Physique des Plasmas, CNRS, Ecole Polytechnique, Sorbonne Université, Université Paris-Saclay, IP Paris, route de Saclay, 91128 Palaiseau, France*
[2)]*ThrustMe, Verrières-le-Buisson, 91370, France*

(Dated: 21 May 2021)

Ion-induced Secondary Electron Emission (SEE) is a fundamental surface interaction that strongly influences many plasma discharges. Recently, interest in iodine plasmas is growing due to new material processing and space propulsion applications, but data for SEE yields due to iodine ion bombardment remains scarce. Additionally, due to the formation of multiple ion species in typical iodine plasmas, and surface chemical reactions leading to iodide layer formation, the effective SEE yield is expected to differ from that for individual ion species on clean surfaces. In this work, we measure the SEE yield of multi-species iodine ion beams bombarding different target materials (Mo, W, Al, Ti, Cu, carbon-carbon, and steel), in the energy range 0.6–1.4 keV. An ion beam is produced by extracting and accelerating ions from a gridded ion source based on an Inductively Coupled Plasma (ICP). SEE yields of downstream targets are measured using a conventional electrostatic probe technique, and the ion beam composition is determined using time-of-flight spectrometry. The beam is composed predominately of atomic (I^+) and molecular (I_2^+) ions whose ratio changes depending on the ICP power. Yields depend strongly on the target material and beam composition, and vary between 0.05-0.4 depending on whether potential or kinetic emission processes dominate.

I. INTRODUCTION

In recent years, iodine has gained increasing attention in the plasma physics and space propulsion communities due to new industrial processes, and the advantages it offers as a propellant for plasma-based propulsion systems, such as gridded ion[1,2], Hall-effect thrusters[3,4] and possibly other systems such as MPD[5] and helicon plasma thrusters[6]. Typically xenon or krypton is used as a propellant for such thrusters due to their inert chemical nature, relatively low ionization energy and high atomic mass (which enhances thruster efficiency and performance). However, these gases are expensive and must be stored in high-pressure tanks, which can create an explosion risk to the launch vehicle and satellite, or require additional certification and insurance. Iodine, on the other hand, is very inexpensive and a solid at room temperature, and can thus be stored unpressurised with a higher density. In addition, iodine has a similar atomic mass and ionization threshold to xenon, making the performance of plasma-based thrusters using iodine similar, or even higher.

Despite numerous experimental[7] and theoretical[8,9] investigations of iodine-based discharges, there is still a lack of fundamental data for many important properties of iodine. Specifically, data for secondary electron emission (SEE) from a material due to iodine ion bombardment is notably scarce. Such SEE data can be important for theoretical and numerical modeling, especially for applications using capacitively coupled plasmas (CCP)[10,11], DC discharges[12,13], and Hall thrusters[14], as well as the analysis of measurements obtained from certain diagnostic probes (such as ion flux probes[15]). As a first effort to improve data availability for iodine-based plasmas, we present an experimental study measuring the SEE yield of an iodine beam bombarding targets made of different materials, specifically: Mo, W, Al, Ti, Cu, carbon-carbon, and steel. Measurements are performed using an iodine ion beam produced by a gridded ion source that uses an Inductively Coupled Plasma (ICP) discharge to generate ions that are then extracted and accelerated by a set of grids.

Compared to noble gases, the measurement of SEE yields due to iodine ion bombardment has two major complications. Firstly, as a halogen, iodine is very reactive which can lead to complex surface chemical reactions with many target materials. Secondly, because iodine gas is mostly stable as a diatomic molecule, plasma discharges produce different ion species (I^+, I_2^+ and I^{2+}), which when accelerated, produce a multi-species ion beam. A number of different SEE studies have been conducted with reactive beams[16–20], mainly focusing on oxygen and nitrogen ion bombardment in the context of reactive sputtering for materials processing. It has been shown that the interaction of these reactive beams, particularly with metallic targets, produces a thin layer of oxides and nitrides. These reaction products directly affect the SEE yield, either increasing or decreasing the yield depending on the specific chemical product present[18]. Because this layer is continuously formed and sputtered in almost any reactive beam or plasma, the SEE yield measured represents an effective yield of the target material and compound layer.

It is important to note that most past experimental works on ion-induced secondary emission have also only focused on the analysis of single-species ion beams, and there is little available information on electron emission due to multi-species beams. However, in the case of beams and plasmas based on molecular gases, the most common situation encountered in different applications is indeed the presence of multiple ion species which may collectively change the surface chemistry and modify the effective SEE yield compared with that observed separately with each species. This is a situation, for example, that would be encountered in many material

[a)]Corresponding author: lui.habl@lpp.polytechnique.fr

processing[21,22] or space propulsion[23,24] applications. Thus, the aim of the present work is not only to provide information on the SEE yield due to iodine ion bombardment, but to also study the emission behavior in the presence of multi-species ion beams. The objective here is to establish an initial estimate of the SEE yield for different target materials to serve as a useful input for future theoretical and numerical modelling.

II. EXPERIMENT

A. Overview

The setup used for the experiments consists of two probes to characterize secondary electron emission from different materials due to the bombardment of an iodine ion beam generated by a gridded ion source. The first and main probe is used to quantify electron emission, and the second probe is used to perform a Time-of-Flight (TOF) spectrometry analysis to estimate the composition of the beam for each secondary electron emission measurement. The arrangement of the experiment is illustrated in figure 1.

The ion beam source used in this work is based on the NPT30 thruster produced by ThrustMe[2]. It consists of a radio-frequency gridded ion source that uses an inductively coupled plasma (ICP) discharge with iodine gas to produce ions that are accelerated by a set of two biased grids, referred to as the screen grid and accel grids respectively. Due to the molecular nature of iodine gas, the plasma in the ICP, and the ion beam propagating downstream, is in general composed of three main ion species: I^+, I_2^+ and I^{2+}, as shown theoretically[8] and experimentally[7]. Because of iodine's electron affinity, negative ions I^- can also be formed in the ICP, however their creation is not favored in the discharge conditions used here[8] and, because of the polarity used and the potential profile of the plasma sheath, the grid set does not extract or accelerate them into the beam.

During the electron emission measurements, the screen grid is biased to voltages between 500 V and 1300 V relative to ground, effectively controlling the final average kinetic energy of the ions, while the accel grid is kept at -100 V to avoid electron backstreaming from the beam. A hot tungsten filament cathode, placed close to the exit of the accel grid, provides the required electron current to ensure quasi-neutrality of the beam. Iodine gas for the discharge is provided by an integrated propellant tank that uses a set of heaters to sublimate solid iodine ($> 99.99\%$ of purity) which is then injected into the ICP discharge cavity. As demonstrated previously[15], the source is capable of providing a beam with 5 to 25 mA of ion current, with a beam divergence half-angle of 8° to 16°.

The beam source, and both probes, are operated within a cylindrical vacuum chamber with a diameter of 0.6 m and a length of 0.83 m. During the experiments, the background pressure is kept below 10^{-5} mbar by using a turbo-molecular and a cryogenic pump connected to the chamber, which provides a pumping speed of 2500 l/s. The probes are positioned at the end of the chamber, close to its back flange, while the beam source is fixed to the center of the front flange. The distance between the source exit plane and the probes is 54 cm. Both probes, described in detail in the sections below, are held by a single metal arm that is fixed to the bottom of the vacuum chamber, with the secondary electron emission probe aligned along the the beam axis, and the TOF probe just below it.

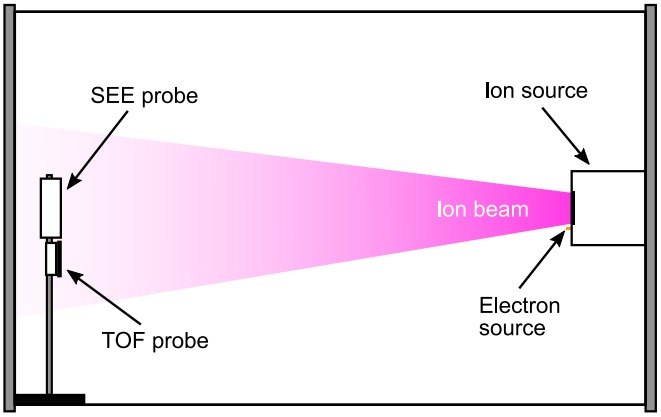

FIG. 1. Side-view schematic of the experiment.

B. Ion-induced secondary electron emission

Measurement of the ion-induced SEE yield is performed using a common method previously described in other experimental works[20]. In this method, the probe is composed of a metallic grid biased to a fixed voltage V_g, and a target electrode made of the material of interest that is biased with a time-varying voltage ramp V_t, and which is bombarded by energetic ions in the beam. A schematic of the SEE probe is shown in figure 2. Whenever $V_t < V_g$, electrons emitted at the target electrode are collected by the grid and the net current measured at the target electrode $I_t(V_t)$ becomes $I_t(V_t < V_g) \approx I_i + I_{SEE}$, where I_i is the collected ion current and I_{SEE} is the current contribution from secondary electrons. On the other hand, when $V_t > V_g$, secondary electrons are reflected and their current is not measured at the target, thus $I_t(V_t > V_g) \approx I_i$. In this way, the current contribution of the secondary electrons can be estimated simply from the difference $I_{SEE} \approx I_t(V_g - \Delta V) - I_t(V_g + \Delta V)$, where ΔV is a given voltage difference. To ensure that the majority of emitted electrons are either reflected or repelled towards the grid, ΔV must be larger than the average kinetic energy at which the secondary electrons are emitted at the target. From the literature[16], this average energy is expected to be of the order of $\langle E_e \rangle \sim 3$eV.

A simplified sectioned view of the SEE probe is shown in figure 2. The outer casing of the probe is made of aluminum and has a cylindrical shape with a diameter of 8 cm and a width of 2.8 cm. The front face of the probe has a circular aperture with a diameter of 2.8 cm through which the ion beam can enter. A grid, made of molybdenum, is placed below the case aperture with a 2 mm vacuum gap. An aluminum spacer ring with a thickness of 2 mm, followed by a 0.2 mm thick mica insulating ring, are placed between the grid and

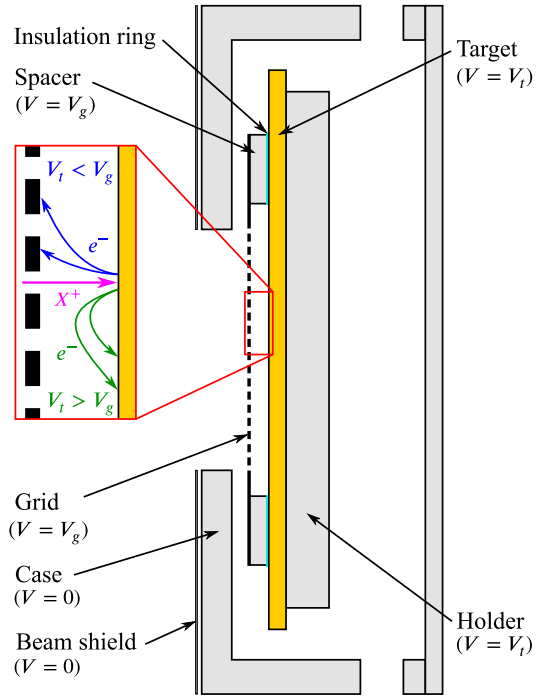

FIG. 2. Schematic showing a sectioned view of the SEE probe. The voltage of each component is written in parenthesis. X^+ represents a generic ion and e^- represents an electron.

the target to ensure their proper spacing. The target material, a square with dimensions of 5 by 5 cm, is placed between the mica ring and an aluminum holder that clamps the target in place. A circular shield is placed in front of the probe covering the aluminum surface (which would otherwise be directly facing the ion beam) to reduce sputtering and avoid arcing due to the possible formation of iodides on the outer casing. The shield is made from molybdenum due to its lower reactivity to iodine[25], and its higher resistance to sputtering compared with aluminum.

During the experiments, the probe is placed within a quasi-neutral ion beam produced by the gridded ion source. To mitigate the effect of the incidence angle of the ions, the probe is axially aligned with the source, favoring ions with velocity vectors aligned perpendicular with the target. Electrons in the beam are emitted from a thermionic neutralizer located near the exit of the ion source. This neutralizer is connected to the vacuum chamber ground, thus ensuring that the beam electrons cannot enter the SEE probe and be collected by the target, which would give rise to an additional undesired electron current. The probe's grid voltage V_g is kept at -100 V during all measurements to stop these electrons. This grid negative bias also prevents the collection of any possible I^- ions which may be generated within the plume during operation.

To estimate the SEE yield of the sample, the target's IV curve is measured, resulting in a step-like curve centered around the grid voltage. This is performed by an external measurement circuit that applies a voltage ramp on the target holder and which measures the current passing through a sense resistor of 1 kΩ using a MCC DT9824 data acquisition

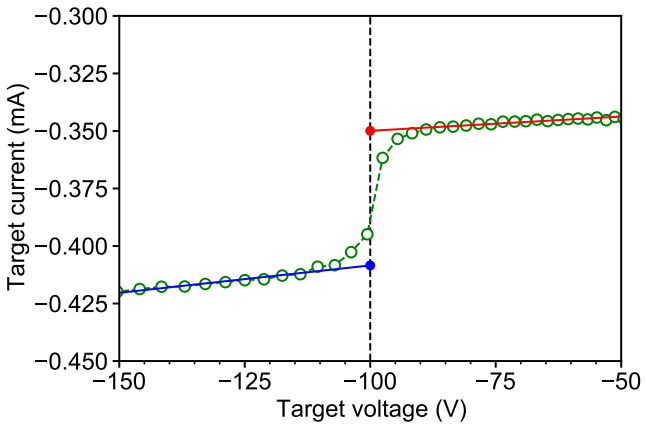

FIG. 3. Example of an IV curve measured with an aluminum target bombarded by a 700 eV beam. The dashed line denotes the probe's grid voltage and the red and blue lines are linear fits to the data before and after the step.

board connected to a computer. The circuit applies a voltage ramp going from -200 V to 5 V in 2 s , which corresponds to approximately 200 recorded points per scan.

Figure 3 shows an example of the measured target current versus voltage for an aluminum sample and a 700 eV beam, with the dashed line showing the grid voltage. The ion current is shown as a negative value to match the usual convention used in IV curves collected with Langmuir probes. It is possible to see that, as expected, for voltages below the dashed line the magnitude of the collected current is higher due to electron escape, and for higher target voltages, electrons are reflected back to the target, hence allowing only the ion current to be measured. A finite slope can also be observed on both "flat" regions of the curve, which ideally should not be present. This can be explained by a combination of two effects: (1) A small leakage current corresponding to an electrical connection of a few tens of mega-ohms to ground, and (2) the penetration of the target potential through the grid, which causes plasma sheath expansion that slightly increases the collection of slow ions present in the beam. To compensate for these effects, instead of taking a fixed voltage step for the estimation of the SEE yield, a linear fit is performed on each "side" of the current step as shown in figure 3. The current values used to calculate the SEE yield are then determined by linear fits with an extrapolation to the grid voltage V_g.

Due to charge-exchange (CEX) collisions of beam ions with the neutral background gas, a population of high-energy neutrals can be formed in the beam which could generate an additional kinetic electron emission on the target, leading to a potential overestimation of the measured yield. A direct measurement of the fast ion flux is non-trivial, and was not performed here due to technical challenges. Nevertheless, we note that the mean free path of CEX collisions, λ_{CEX}, in the present experimental conditions is expected to be much larger than the distance from the source to the SEE probe. Because of a lack of reliable cross-section data for iodine available in the literature, it is possible to make a first approxi-

mation of λ_{CEX} using cross-sections for xenon[26], which gives $\sigma \approx 6.6 \times 10^{-19}\mathrm{m}^2$ for 1 keV ions. Considering an average pressure of 10^{-5} mbar, we find $\lambda_{CEX} \approx 7$m, which approximately one order of magnitude higher than the vacuum chamber length. If one considers that $G_n = (1 - \exp[-x/\lambda_{CEX}])$, where G_n is the ratio of the beam particles that suffered collisions and x is the distance travelled by the beam, the final particle flux would be composed of roughly 7% fast neutrals. However, there is also the effective transparency of the grid and loss of focusing of these fast neutrals through the probe (since they are uncharged), which will decrease the neutral flux bombarding the sample further. Thus, this estimate represents an upper limit. In this way, we expect a relatively low impact in the measurements of the SEE yield due to fast neutrals.

Both diatomic and monoatomic iodine are strongly reactive with a large range of materials, including some of the targets used here[25,27]. Because of this, it is expected that the beam and background neutral gas react with the surface of the samples to form a thin layer of iodide compounds, which may have very different SEE yield coefficients when compared with a clean surface. On the other hand, during the measurements, the samples are constantly cleaned by the bombardment of high-energy ions which partially removes these reaction products. The balance between surface reactions and ion cleaning should yield a constant thickness layer at steady state. Corbella et al.[20] performs a similar experiment but for an oxygen beam interacting with titanium and aluminum samples, and concludes that the reactions producing the oxide layer happen only in the first atomic monolayers of the sample producing an oxidized layer with a thickness of the order of 5 nm. It is beyond the scope of this article to study all iodine reactions taking place on the surface of the samples, so we report here only measurements of the effective SEE yields of the possibly partially iodized samples. Nevertheless, since these surface reactions would likely happen in almost every application of iodine beams and plasmas, the experimental points measured here provide a good estimation of the electron emission even without the specific details of the iodide layer formed.

C. Beam composition

As discussed previously, the ion beam produced by the source contains different iodine ion species, namely I^+, I_2^+ and I^{2+}. Each of these ions may lead to different electron emission behavior on impact, thus it was necessary to characterize the composition of the beam during each SEE measurement. To accomplish this, a Time-of-Flight (TOF) spectrometry technique[28] was employed to determine the beam composition, and understand the influence of each species on the SEE measurements.

The TOF measurements were made using a circular molybdenum probe with a diameter of 7 cm placed 54 cm from the exit plane of the ion source. To perform the TOF measurement, both the screen and acceleration grids of the source are initially grounded before a rectangular voltage pulse of approximately 4.5 µs and 1 kV is applied to the screen grid, forming a group of approximately monoenergetic particles. Because of their different charge-to-mass ratios, the particle groups arrive at the probe at different times, generating distinct current peaks. A digital oscilloscope was used to measure the current collected by the probe, which was then integrated to estimate the contribution from each type of ion. To decrease the collection of beam electrons and any possible I^- ions formed in the beam, the probe was kept at -100 V during all measurements.

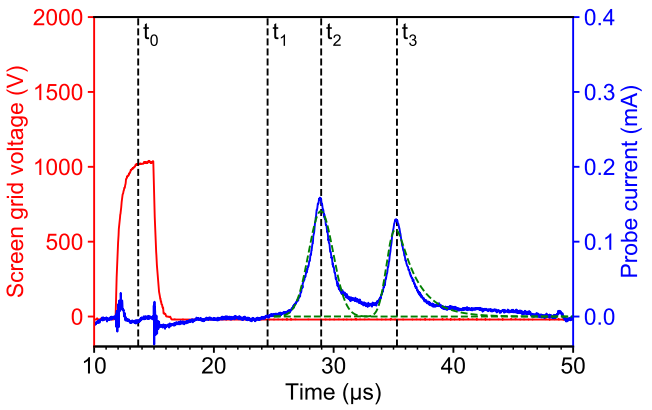

FIG. 4. Example of a TOF measurement showing the current collected by the probe (blue) and the voltage pulse applied to the source grid (red). The time t_0 represents the time of the center of the pulse, and t_1, t_2 and t_3 are the theoretical travel times of I^{2+} I^+ and I_2^+ respectively. The dashed curves (green) are curve fits to the main peaks appearing in the signal.

Figure 4 shows an example of a measurement performed with the TOF probe. The red curve shows the acceleration voltage pulse applied to the screen grid of the source, while the blue curve is the current collected by the probe. Each current peak corresponds to a different species and it is possible to estimate their relative concentration by calculating the integral value of each peak. The dashed vertical lines represent the theoretical travel times of each particle species if they were monoenergetic at the average voltage of the grid voltage pulse, where t_0 is the time of the center of the pulse, and t_1, t_2 and t_3 are transit times for I^{2+} I^+ and I_2^+ respectively. No measurable peak corresponding to I^{2+} was observed in any TOF measurements performed during this work, so only I^+ and I_2^+ are considered below. Furthermore, because of limitations on the physical length of the drift region of the experiment and on the width of the pulse, the individual peaks are not clearly separated but have a certain degree of overlap between them. To account for this spread, each peak was fitted with an exponential Gaussian curve, as shown by the green dashed curves in the figure. For this specific measurement, the relative composition of I^+ and I_2^+ is estimated to be approximately 52% and 48% respectively. Using the TOF apparatus, the SEE yield for every material is characterized for two distinct beam modes with different relative beam compositions.

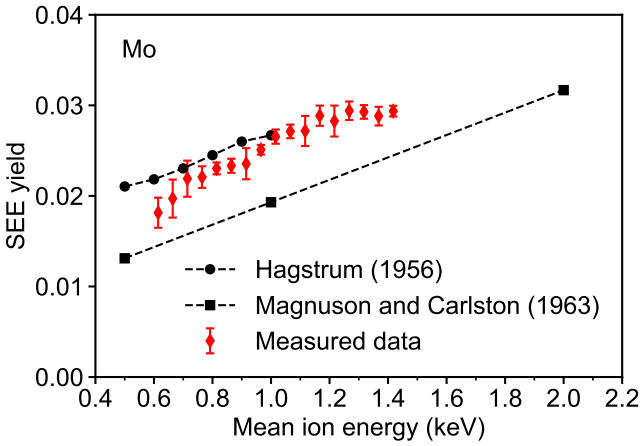

FIG. 5. SEE yield of a molybdenum target as a function of the mean ion bombarding energy of a xenon beam. The data is compared with previous measurements in Ref. 29 and Ref. 30.

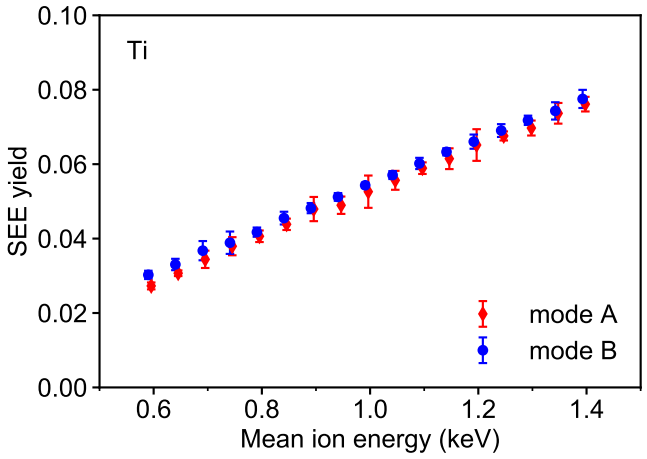

FIG. 6. Effective SEE yield of a titanium target as a function of the mean ion bombarding energy. The data is measured for two different beam composition conditions, mode A and mode B, which are described in table II.

TABLE I. Materials used as target samples in the electron emission experiment.

Material	Manufacturer	Composition
Molybdenum (Mo)	Goodfellow	Mo > 99.9%
Tungsten (W)	Goodfellow	W > 99.9%
Aluminum (Al)	Goodfellow	Al > 99.0%
Titanium (Ti)	Goodfellow	Ti > 99.6%
Copper (Cu)	Goodfellow	Cu > 99.9%
Carbon-carbon (CC)	Goodfellow	Unspecified
Steel	Precision Brand	AISI 1008

D. Target materials and experimental procedure

The central objective in the experiments is to measure the SEE yield of different targets while computing the relative ion species composition of the beam bombarding the sample. The materials used are summarized in table I, and all samples are polycrystalline. Before installation in the SEE probe, each sample went through the same cleaning procedure to mitigate undesired effects due to other possible deposited materials. Each sample is cleaned superficially and placed for 15 minutes inside an ultrasonic bath with ethanol. After this, and immediately before the measurements, the sample is exposed to the iodine ion beam for 20 minutes at 1 keV to further clean the surface of the target, as typically done for SEE yield measurements[31], and induce any surface chemical reactions (which would be present in any realistic iodine plasma application) that might take place during the bombardment to avoid transient processes during the measurements.

To investigate the influence of each ion species, the SEE yield measurement for each material is divided into two phases. In the first phase the ion source is operated in a low-power mode, called mode A, that produces a beam composition where the proportion of I^+ and I_2^+ is similar with a ratio of approximately 50:50; while for the second phase, the source is operated in a high-power mode, denoted mode B, which generates a discharge dominated by I^+ with a ratio of approximately 75:25. Mode B also favors the production of I^{2+}, however its concentration was found to be less than 1% in both modes, so its influence is expected to be much less pronounced than for the other two species. With the TOF probe, the composition of the beam is assessed before each phase of the SEE measurement.

For each mode, the SEE yield is measured for different ion energies, between 0.6 keV and 1.4 keV with steps of 50 V. For this setup, the average ion energy can be approximated by $\langle E_i \rangle \approx V_p + V_s - \langle V_c \rangle$, where V_p is the ICP plasma potential, V_s is the screen grid voltage, and $\langle V_c \rangle$ is the average voltage of the SEE probe collector close to moment of the current step used for the measurement. Because $V_p \ll V_s$ and $\langle V_c \rangle \approx -100$V, the ion bombarding energy is estimated as $\langle E_i \rangle \approx V_s + 100$V. For every energy step, approximately 20 voltage scans in the target are executed and measured. The emission yield is then estimated for every individual IV curve using the curve fitting method described above. Lastly, the set of measured yields for each energy step is averaged, which provides a mean SEE yield curve as a function of beam energy.

To verify that the method used here provides realistic results, the probe was used to measure the SEE yield of xenon ions bombarding a molybdenum target. Figure 5 shows the results obtained. The measured values are compared with the independent data obtained by Hagstrum[29] and Magnuson and Carlston[30], which shows relatively good agreement.

III. RESULTS AND DISCUSSION

The results of the SEE and TOF measurements are presented here for each of the target materials. Figure 6 shows the measurement of the SEE yield for the titanium target as a function of the mean ion bombarding energy. Each point on the plot corresponds to an average value of several yields

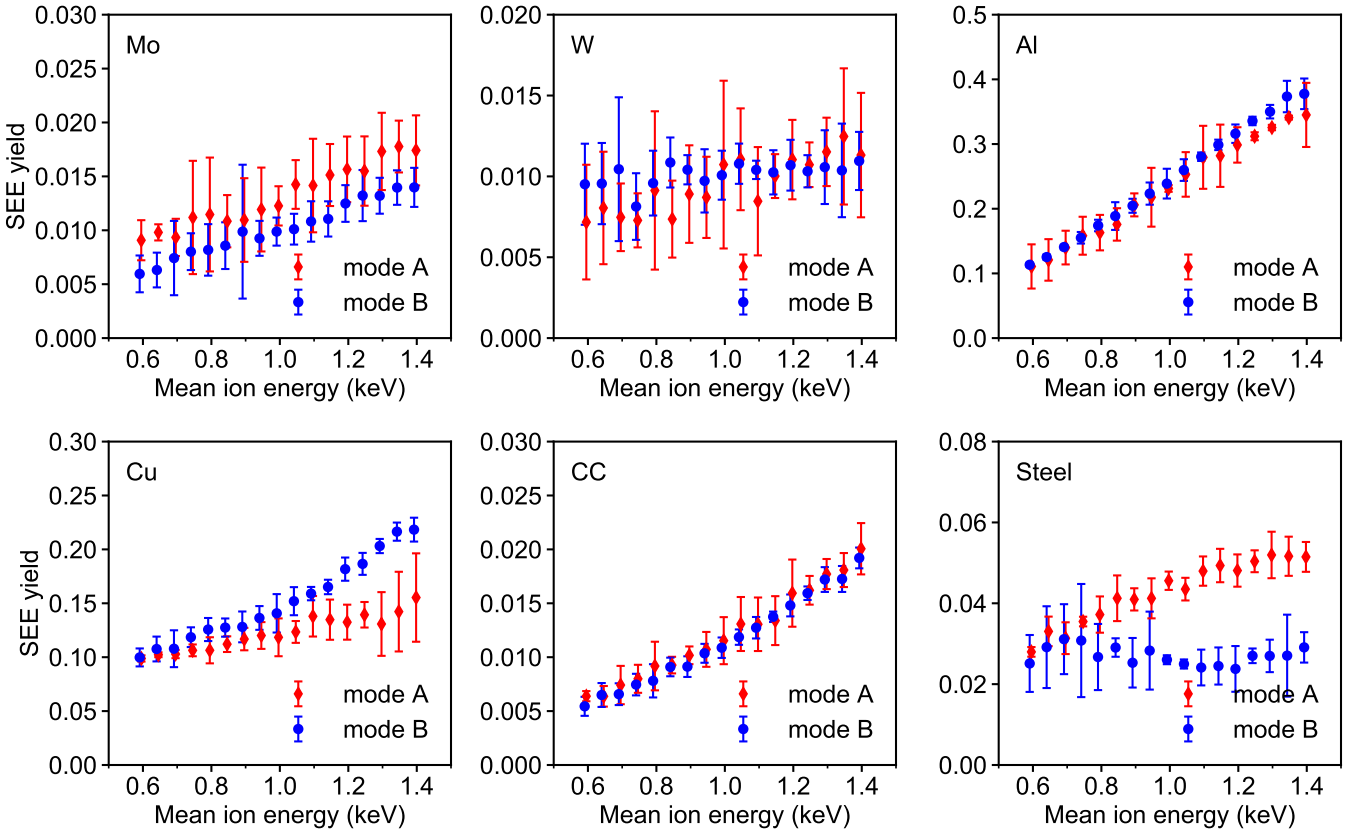

FIG. 7. Effective SEE yield for different target materials as a function of the mean ion bombarding energy. The data is measured for two different beam composition conditions, mode A and mode B, which are detailed in table II.

TABLE II. Relative concentration of I^+ and I_2^+ ions in the beam, measured with the TOF probe before each SEE measurement.

	Mode A		Mode B	
Target	I^+	I_2^+	I^+	I_2^+
Mo	0.567	0.433	0.760	0.240
W	0.515	0.485	0.754	0.246
Al	0.495	0.505	0.739	0.261
Ti	0.531	0.469	0.740	0.260
Cu	0.572	0.428	0.761	0.239
CC	0.544	0.456	0.767	0.233
Steel	0.556	0.444	0.751	0.249

determined from all the voltage scans performed at each ion energy step; the error bar interval for each point corresponds to the standard deviation of each group of yields used to determine them. The data is displayed for both beam modes, which have their relative ion species composition displayed in table II. As can be seen from the graph, the effective SEE yield in the energy range studied monotonically increases from about 3% to 8%. An important observation is that the SEE yields measured with both beam modes are similar, suggesting that the emission behavior due to bombardment of either I^+ or I_2^+ is similar despite the difference in the charge-to-mass ratio and ionization potential of each species.

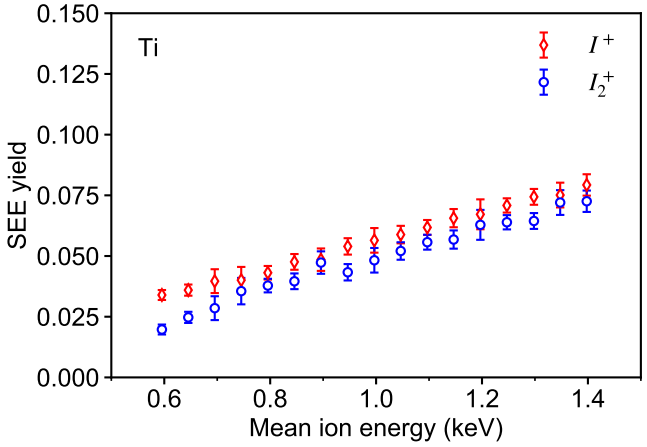

FIG. 8. Estimated individual SEE yield of an titanium target for each ion species as a function of the mean ion bombarding energy. The data is estimated using the relative composition measured with the TOF apparatus detailed in table II.

As described in detail in Ref. 32, two main, and distinct, emission mechanisms take place in ion-induced SEE: potential emission and kinetic emission. In potential emission, an electron is excited and ejected due to the transfer of inter-

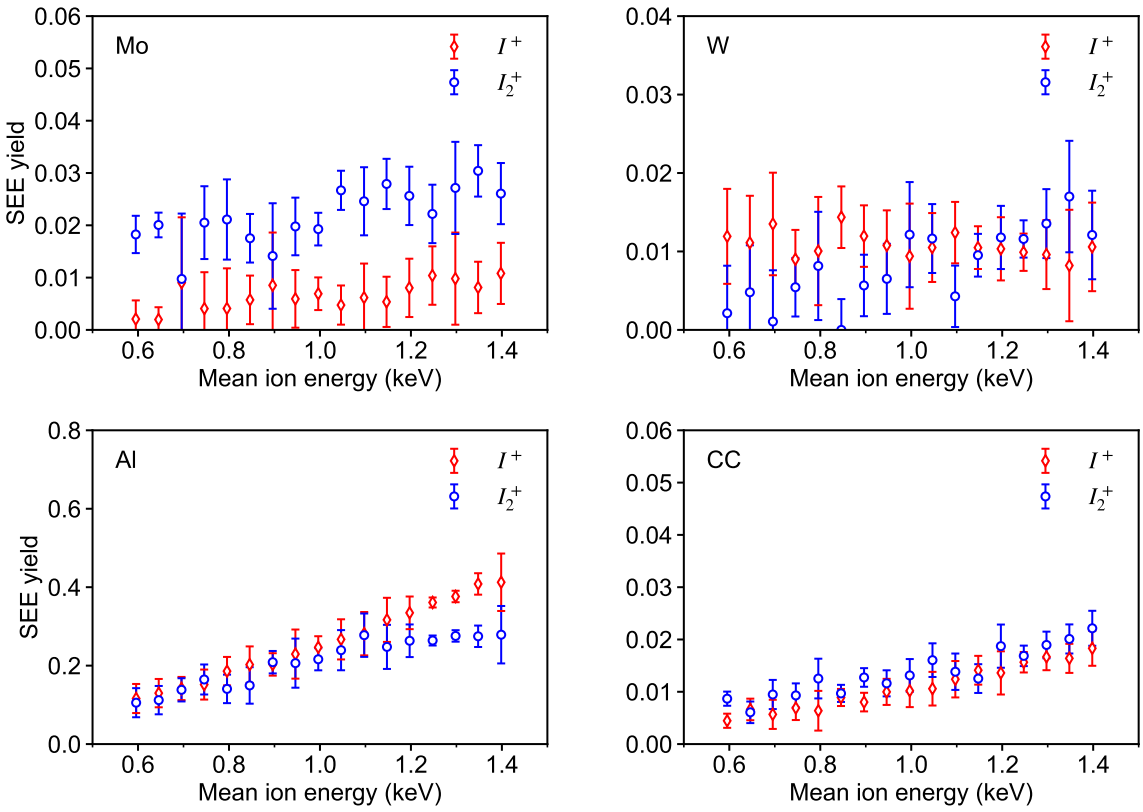

FIG. 9. Estimated individual SEE yield for different target materials for each ion species as a function of the mean ion bombarding energy. The data is estimated using the relative composition measured with the TOF apparatus detailed in table II.

nal energy of the incident ion to the electron in the so-called Auger process. In this case, the emission yield is independent of the incoming ion kinetic energy. On the other hand, with kinetic emission, electrons are ejected due to kinetic energy transfer during the collision, and thus, in this case, the SEE yield typically has a strong dependence on the ion energy. The threshold between both mechanisms is usually of the order of a few hundred electronvolts for clean metals, however, the determination of a precise threshold value is challenging. In the case of the almost linear SEE yield dependence with ion energy seen in figure 6, kinetic emission likely dominates over potential emission in this case[17].

Figure 7 shows the results of the emission measurements for all other sample materials. For the case of Mo, W and CC the variation of the yield as a function of ion energy is relatively small compared with the other materials, showing that in these cases, the effect of potential emission likely dominates. Because the magnitude of the SEE yield is much smaller for these materials, the signal-to-noise ratio is also reduced, thus making the error bars more significant. Like Ti, Al also shows a linear dependence with ion energy, again consistent with kinetic emission.

In the specific case of copper and steel, it is possible to observe a unique behavior not consistent with the other materials, where the SEE yields measured for both beam modes do not coincide. These results were at least partially confirmed with repeated measurements with different times of initial exposure to the beam before each measurement cycle, indicating that this behavior was not due to chemical transient processes. This behavior is still not well understood, but is expected to be a direct consequence of the formation of compounds such as CuI and FeI_2, on the surface of the samples. The formation of compounds is less favored in the case of Mo, W, Ti and CC, and it is expected to happen at a higher rate for Cu, steel, and Al[25]. Generally, it is observed that for the less reactive targets, the SEE yields are lower and similar for both modes. For the rest of the materials (which are generally more reactive with iodine), the magnitude of the SEE yield is higher and shows a clear difference for both modes.

Typically, it is also possible to analyze the first derivative of the measured IV curves to estimate the electron energy distribution function and verify if any changes in the work function of the material, or the emission characteristics, have occurred[16]. Performing the first derivative of the IV curves measured in the present work, it was found that the distribution functions at each ion bombarding energy were similar and no significant shift was observed, thus indicating that the material and emission properties do not change appreciably.

Using the effective SEE yields obtained for Mode A and Mode B, and the relative composition of the beam, it is possible to estimate the individual SEE yield of each ion species assuming that the measured effective value is a linear superposition of the emission of each species: $\gamma_{\text{eff}} = \bar{n}_{I^+}\gamma_{I^+} + \bar{n}_{I_2^+}\gamma_{I_2^+}$,

where $\bar{n}_{I^+}$ and $\bar{n}_{I_2^+}$ are the relative composition of each species given in table II, and, γ_{I^+} and $\gamma_{I_2^+}$ are the individual yields to be estimated. It is important to note that this assumption does not capture the effect of a change in surface chemistry caused by each species which may be important and lead to a different functional relationship depending on the beam composition. Using a non-negative least square method, the individual SEE yields are estimated for each energy step separately and the result is presented in figure 8 for Ti. The error bars in the individual yield estimation is assumed to be the sum of the errors of the effective yield measurements. It is possible to see that the individual yields are similar to the effective yield, and the atomic ion gives a slightly higher yield than the molecular ion. For potential emission, a higher ionization energy is expected to give a higher yield, which is consistent with the results in figure 8 since I^+ has a higher ionization threshold than I_2^+. Similar behavior has been seen previously with atomic and diatomic nitrogen and oxygen ions[33].

Figure 9 shows the individual SEE yields for the other materials. The plots for copper and steel are omitted from this figure because the quality of their estimated individual yields is too poor for any practical use. For the other targets, the individual SEE yields are close to the effective SEE yields presented above. We also note that for some materials the individual SEE yield of I_2^+ is higher than I^+, which is unexpected when considering potential emission as I^+ has a higher ionization threshold than I_2^+. This behavior most likely results from a change in the surface state of the samples due to chemical reactions with iodine.

IV. CONCLUSION

In this work, we have measured the ion-induced SEE yield of different materials bombarded by iodine ions. To perform these measurements, a special probe was constructed that consists of a biased front grid, and a biased target. By varying the voltage between the grid and the target, it was possible to control whether any emitted electrons escape, or are collected by the target, which allows a measurement of the SEE yield. Because the ion source used produces a multi-species ion beam composed primarily of I_2^+ and I^+, an in-situ TOF method was employed to measure the relative composition of the beam. To verify the influence of these different species, the effective SEE yield values for each material were measured in two distinct beam modes with I^+ and I_2^+ current ratios of about 50:50 and 75:25 respectively.

It was observed that the composition of the beam plays only a minor role for five of the seven materials tested (i.e. Ti, Mo, W, CC, and Al). By contrast, the SEE yield varies significantly with beam composition for Cu and steel. The exact reason for this is not yet known, but is most likely due to chemical surface reactions producing a thin iodide layer that changes the SEE yield. In any case, these reactions are intrinsic to the operation of iodine-based beams and plasmas with such materials, and hence the effective SEE yield may represent a more relevant value than the SEE yields for each individual ion species on a clean surface. It was also observed that with some samples, such as Ti, Al, and CC, the SEE yield is similar for both beam modes tested, and varies linearly with ion energy. This suggests that kinetic emission dominates in the regime studied here.

There are a few points that require clarification and careful study in future investigations. In particular, a better understanding of relevant surface chemical reactions is needed, as well as the characterization of any iodide layers that form, and how these layers modify the SEE yield. As such chemical reactions, and any iodide layer thickness, is expected to depend on the ion bombarding energy, a wider range of ion energies may be needed to better understand the variation in SEE yield with surface state, and more clearly study the transition from potential to kinetic emission.

ACKNOWLEDGMENTS

This work was partly funded by the European Commission's Horizon 2020 research and innovation program under grant agreement No. 823337, and ANRT with a Cifre scholarship awarded to LH. The authors would like to thank and acknowledge Ane Aanesland for support, and a number of technical discussions.

DATA AVAILABILITY

The data that support the findings of this study are available from the corresponding author upon reasonable request.

 This article appeared in L. Habl, D. Rafalskyi, and T. Lafleur,"Secondary electron emission due to multi-species iodine ion bombardment of different target materials," Journal of Applied Physics, vol. 129, no. 15, p. 153302, Apr. 2021, doi: 10.1063/5.0048447 and may be found at `https://doi.org/10.1063/5.0048447`.

REFERENCES

[1] K. Holste, W. Gärtner, D. Zschätzsch, S. Scharmann, P. Köhler, P. Dietz, and P. J. Klar, "Performance of an iodine-fueled radio-frequency ion-thruster," The European Physical Journal D **72**, 9 (2018).

[2] J. Martinez Martinez, D. Rafalskyi, and A. Aanesland, "Development and testing of the NPT30-I2 iodine ion thruster," in *36th International Electric Propulsion Conference* (2019).

[3] J. Szabo, B. Pote, S. Paintal, M. Robin, A. Hillier, R. D. Branam, and R. E. Huffmann, "Performance evaluation of an iodine-vapor hall thruster," Journal of Propulsion and Power **28**, 848–857 (2012).

[4] H. Kamhawi, T. Haag, G. Benavides, T. Hickman, T. Smith, G. Williams, J. L. Myers, K. A. Polzin, J. Dankanich, L. Byrne, *et al.*, "Overview of iodine propellant hall thruster development activities at nasa glenn research center," in *52nd AIAA/SAE/ASEE Joint Propulsion Conference* (2016) p. 4729.

[5] A. Sasoh and Y. Arakawa, "Electromagnetic effects in an applied-field magnetoplasmadynamic thruster," Journal of Propulsion and Power **8**, 98–102 (1992).

[6]K. Takahashi, "Helicon-type radiofrequency plasma thrusters and magnetic plasma nozzles," Reviews of Modern Plasma Physics **3** (2019), 10.1007/s41614-019-0024-2.

[7]P. Dietz, W. Gärtner, Q. Koch, P. E. Köhler, Y. Teng, P. R. Schreiner, K. Holste, and P. J. Klar, "Molecular propellants for ion thrusters," Plasma Sources Science and Technology **28**, 084001 (2019).

[8]P. Grondein, T. Lafleur, P. Chabert, and A. Aanesland, "Global model of an iodine gridded plasma thruster," Physics of Plasmas **23**, 033514 (2016).

[9]R. Lucken, F. Marmuse, A. Tavant, A. Bourdon, and P. Chabert, "Global model of a magnetized ion thruster with xenon and iodine," in *36th International Electric Propulsion Conference*, IEPC-2019-678 (2019).

[10]T. Lafleur, P. Chabert, and J. P. Booth, "Secondary electron induced asymmetry in capacitively coupled plasmas," Journal of Physics D: Applied Physics **46**, 135201 (2013).

[11]Y.-Y. Wen, Y.-R. Zhang, G. Jiang, Y.-H. Song, and Y.-N. Wang, "Secondary electron effect on sustaining capacitively coupled discharges: A hybrid modeling investigation of the ionization rate," AIP Advances **9**, 055019 (2019).

[12]M. Radmilović-Radjenović and B. Radjenović, "A particle-in-cell simulation of the breakdown mechanism in microdischarges with an improved secondary emission model," Contributions to Plasma Physics **47**, 165–172 (2007).

[13]Z. Donkó, "Apparent secondary-electron emission coefficient and the voltage-current characteristics of argon glow discharges," Physical review E **64**, 026401 (2001).

[14]I. D. Kaganovich, Y. Raitses, D. Sydorenko, and A. Smolyakov, "Kinetic effects in a hall thruster discharge," Physics of Plasmas **14**, 057104 (2007).

[15]L. Habl, D. Rafalskyi, and T. Lafleur, "Ion beam diagnostic for the assessment of miniaturized electric propulsion systems," Review of Scientific Instruments **91**, 093501 (2020).

[16]Y. Yamauchi and R. Shimizu, "Secondary Electron Emission from Aluminum by Argon and Oxygen Ion Bombardment below 3 keV," Japanese Journal of Applied Physics **22**, L227–L229 (1983).

[17]M. A. Lewis, D. A. Glocker, and J. Jorne, "Measurements of secondary electron emission in reactive sputtering of aluminum and titanium nitride," Journal of Vacuum Science & Technology A: Vacuum, Surfaces, and Films **7**, 1019–1024 (1989).

[18]D. Depla, X. Y. Li, S. Mahieu, and R. De Gryse, "Determination of the effective electron emission yields of compound materials," Journal of Physics D: Applied Physics **41**, 202003 (2008).

[19]A. Marcak, C. Corbella, T. de los Arcos, and A. von Keudell, "Note: Ion-induced secondary electron emission from oxidized metal surfaces measured in a particle beam reactor," Review of Scientific Instruments **86**, 106102 (2015).

[20]C. Corbella, A. Marcak, T. de los Arcos, and A. von Keudell, "Revising secondary electron yields of ion-sputtered metal oxides," Journal of Physics D: Applied Physics **49**, 16LT01 (2016).

[21]D. Flanders, L. Pressman, and G. Pinelli, "Reactive ion etching of indium compounds using iodine containing plasmas," Journal of Vacuum Science & Technology B: Microelectronics Processing and Phenomena **8**, 1990–1993 (1990).

[22]A. Wright, "Artefacts in iodine ion milling of some compound semiconductors," Ultramicroscopy **83**, 1–8 (2000).

[23]J. Szabo and M. Robin, "Plasma species measurements in the plume of an iodine fueled hall thruster," Journal of Propulsion and Power **30**, 1357–1367 (2014).

[24]Z. R. Taillefer, J. J. Blandino, and J. Szabo, "Characterization of a barium oxide cathode operating on xenon and iodine propellants," Journal of Propulsion and Power **36**, 575–585 (2020).

[25]K. A. Polzin, S. R. Peeples, J. F. Seixal, S. L. Mauro, B. L. Lewis, G. A. Jerman, D. H. Calvert, J. Dankanich, H. Kamhawi, T. A. Hickman, J. Szabok, B. Pote, and L. Lee, "Propulsion system development for the iodine satellite (iSAT) demonstration mission," in *34th International Electric Propulsion Conference* (2017).

[26]A. V. Phelps, "Phelps database," `http://jilawww.colorado.edu/~avp/` (2020).

[27]J. Martinez Martinez and D. Rafalskyi, "Development of iodine propellant and flow control units suitable for multiple propulsion systems," in *Space Propulsion Conference* (2020).

[28]V. Gushenets, A. Nikolaev, E. Oks, L. Vintizenko, G. Y. Yushkov, A. Oztarhan, and I. Brown, "Simple and inexpensive time-of-flight charge-to-mass analyzer for ion beam source characterization," Review of scientific instruments **77**, 063301 (2006).

[29]H. D. Hagstrum, "Auger Ejection of Electrons from Molybdenum by Noble Gas Ions," Physical Review **104**, 672–683 (1956).

[30]G. D. Magnuson and C. E. Carlston, "Electron Ejection from Metals due to 1- to 10-keV Noble Gas Ion Bombardment. I. Polycrystalline Materials," Physical Review **129**, 2403–2408 (1963).

[31]J. Ferron, E. V. Alonso, R. A. Baragiola, and A. Oliva-Florio, "Electron emission from molybdenum under ion bombardment," Journal of Physics D: Applied Physics **14**, 1707–1720 (1981).

[32]R. A. Baragiola and P. Riccardi, "Electron Emission from Surfaces Induced by Slow Ions and Atoms," in *Reactive Sputter Deposition*, Vol. 109, edited by R. Hull, R. M. Osgood, J. Parisi, H. Warlimont, D. Depla, and S. Mahieu (Springer Berlin Heidelberg, Berlin, Heidelberg, 2008) pp. 43–60.

[33]P. Mahadevan, G. D. Magnuson, J. K. Layton, and C. E. Carlston, "Secondary-Electron Emission from Molybdenum Due to Positive and Negative Ions of Atmospheric Gases," Physical Review **140**, A1407–A1412 (1965).